Environmental Science & Technology

pubs.acs.org/est

Article

Organophosphate Ester Migration Mechanisms and Environmental Impacts in the Western South China Sea

Published as part of Environmental Science & Technology special issue "Ocean Health".

Minwei Han, Kefu Yu,* Ruijie Zhang, Biao Chen, Mei Xiong, Yaru Kang, Xiaopeng Yu, Zhenjun Qin, and Xiangrong Xu

Cite This: https://doi.org/10.1021/acs.est.5c09148

Read Online

ACCESS | Metrics & More | Article Recommendations | Supporting Information

ABSTRACT: Organophosphate esters (OPEs) are ubiquitous in various environmental media and are of concern because of their toxicity and potential ecological impacts. However, their transport mechanisms and ecological effects in marine environments remain poorly understood. Herein, we comprehensively investigated the occurrence and distribution of OPEs in multiple environmental media (atmosphere, rainwater, seawater, and sediments) in the western South China Sea (WSCS). Results show that OPEs are widespread in the WSCS. OPE concentrations in the atmosphere were higher than those reported in most other marine regions globally, whereas concentrations in seawater were either lower than or comparable to those in other oceanic regions. The biogeochemical cycling of OPEs is driven primarily by particulate matter (PM) and microbial activity. PM facilitates the transport of 65.3−98.4% of total OPEs and 60.5−100% of chlorinated OPEs from the atmosphere to the ocean. PM sinking strongly influences the vertical distribution of OPEs, while microorganisms contribute to OPE biodegradation through community succession, differentiation of ecological niches among key functional groups, and hydrolytic enzyme activity. Given the increasing concentrations of OPEs in the South China Sea, it is imperative to conduct comprehensive and continuous investigations of their migration mechanisms and impacts on marine ecosystems, particularly coral reefs.

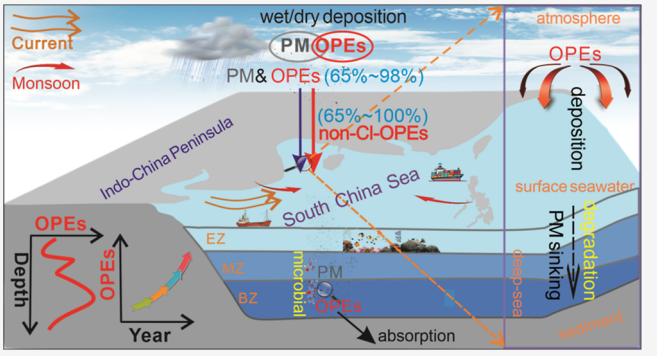

KEYWORDS: *organophosphate esters, environmental behavior, migration mechanisms, particulate matter, microbial activity*

1. INTRODUCTION

Organophosphate esters (OPEs) are widely used as flame retardants in polymers,[1,2] plasticizers,[3] defoamers[4] in various commercial and industrial products. Their production and use inevitably result in the release of residual OPEs into environmental media. Trace levels of OPEs have been detected in remote oceans, including the Southern Ocean and the polar regions.[1,5] The high lipophilicity of OPEs is of particular concern because it facilitates their accumulation in marine organisms such as corals, fish, and shellfish, and their subsequent transfer along the food chain, potentially posing threats to ecosystems and human health.[6−8]

The atmosphere influences the transport and distribution of OPEs in the environment, and the ocean is considered an important reservoir for these compounds.[1] The widespread distribution of OPEs in various environmental media underscores their considerable environmental transport properties.[7,9] Concurrently, their potential biotoxicity, including endocrine disruption abilities, neurotoxicity, reproductive toxicity, and carcinogenicity, is of high concern.[3,9] Remote marine environments are geographically distant from the direct impact of large-scale human activities and industrialized urban production. However, pollutants frequently enter the marine environment through multiple pathways, including atmospheric transport, riverine input, rainfall, and particulate matter (PM) deposition.[10,11] Under conditions of global warming and ocean acidification, these inputs may further exacerbate ecological threats to sensitive marine ecosystems such as coral reefs.[12,13] The biogeochemical cycling of OPEs in the marine environment is influenced by multiple factors, including their physical and chemical properties, ocean currents, atmospheric circulation, solar radiation, marine biological pumps (MBLPs), microbial activity, and particle deposition, leading to variations in their

Received: July 7, 2025
Revised: October 15, 2025
Accepted: October 15, 2025
Published: October 20, 2025

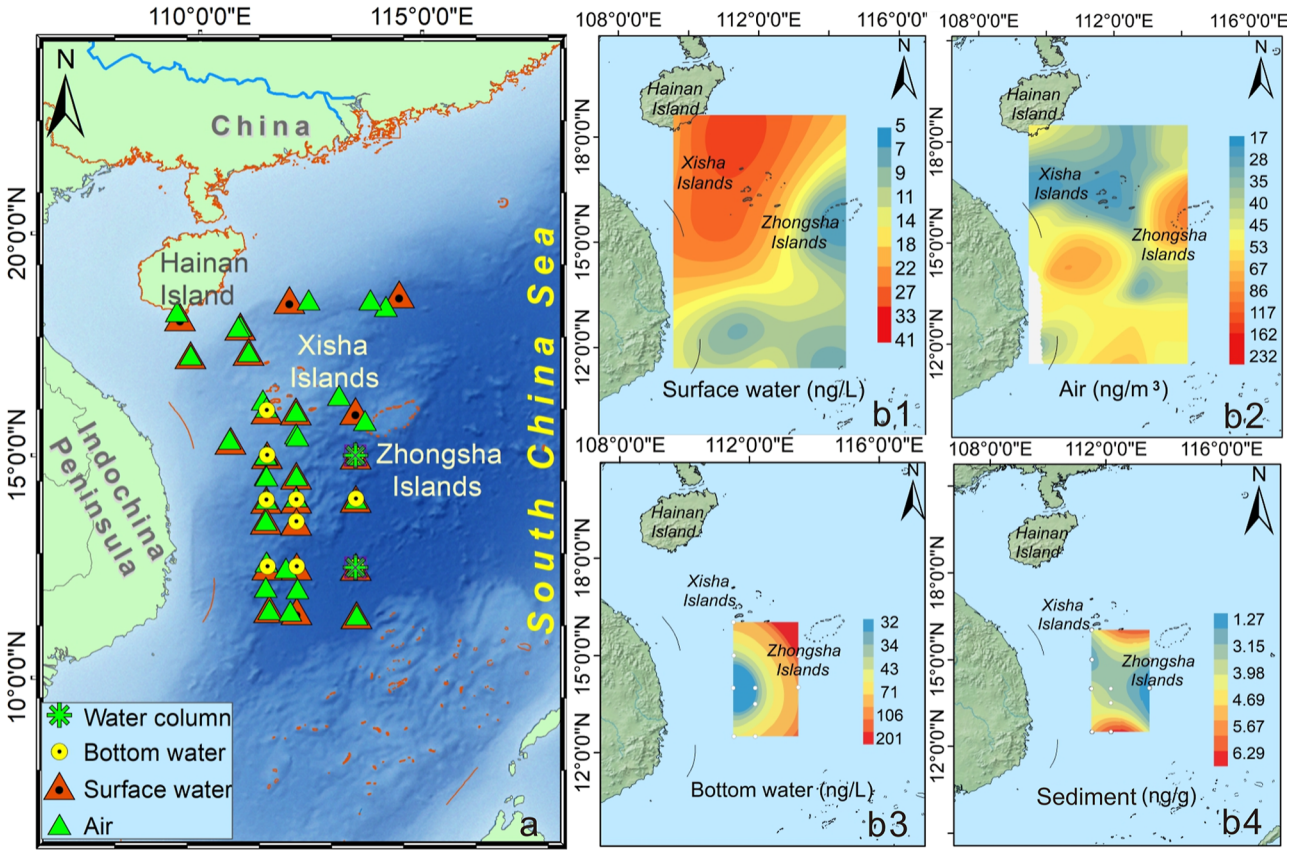

Figure 1. Sampling points (a) and distribution characteristics of OPEs (b) during the voyage in the WSCS.

behavior across different environmental media.[1,14−16] The diffusion patterns of ocean currents and sinking behavior of PM facilitate the diffusive transportation of semivolatile organic compounds (SVOCs) in surface systems and also impact their distribution and environmental behaviors within deep-sea systems.[17,18] The western South China Sea (WSCS) is influenced by intensive shipping activities and land-based runoff and is also impacted by the summer monsoon of the South China Sea (SCS). Pollution from shipping activities and rivers (e.g., Pearl and Mekong rivers) is transported into the SCS via diffusion with ocean currents,[19] and the terrigenous sources of SVOCs originating from excess human activities eventually end up in the SCS via the long-range transportation (LRT) of the atmosphere from land sources such as the Indochina Peninsula and Luzon Island.[20,21] The SCS is characterized by the presence of numerous coral reefs, which have been recognized for their remarkable biodiversity. However, currently, they are experiencing incessant bleaching and deterioration.[22] In the context of climate change, the damage to coral reefs due to intensified human activities appears to be more prominent, and the adverse effects of SVOCs on coral reefs are especially concerning. The deleterious effects of these pollutants on coral reefs predominantly include the destruction of coral symbiotic organisms, impacts on photosynthesis, changes in reef nutritional patterns, induction of oxidative stress, and inhibition of growth.[23−27] The WSCS serves as a transition zone for the migration of land-based pollution to coral reef regions of the SCS and is perennially exposed to various human activities, including terrestrial pollution, riverine input, and shipping.[17,19,28] However, the current status of OPE pollution and their environmental behavior in the region remain poorly understood, and the driving mechanisms of their biogeochemical cycling processes and ecological impacts are still unclear.

Therefore, this study aims to (1) quantify the occurrence and spatiotemporal trends of OPEs across multiple environmental compartments in the WSCS; (2) elucidate the vertical transport mechanisms of OPEs from the atmosphere to the ocean interior, including deep-sea systems; and (3) identify the key drivers governing the distribution and fate of OPEs in ocean vertical profiles. Collectively, these findings will advance understanding of the biogeochemical cycling, underlying mechanisms, and potential ecological impacts of OPEs as emerging contaminants in the marine environment.

2. MATERIALS AND METHODS

2.1. Chemicals and Reagents. Eleven widely used OPEs, including three chlorinated OPEs (Cl-OPEs) and eight nonchlorinated OPEs (non-Cl-OPEs), were selected as target compounds in this study. Their detailed physicochemical properties are provided in Text S1 and Table S1.

2.2. Sampling and Sample Pretreatment. All samples were collected during a cruise aboard the research vessel Xiangyanghong 3 in August 2021 (Figure 1). For the investigation of OPE concentrations, air, surface seawater, water column, bottom water, rainwater, and sediment samples (Tables S3−S6) were collected as described in our previous study.[17] In brief, atmospheric samples were collected using an active atmospheric sampler. Surface seawater was collected and passed through glass fiber filters (GFFs) and two tandem polyurethane foam (PUF) columns to enrich particle- and dissolved-phase OPEs. All the water column, bottom water, and rainwater samples were collected in brown glass bottles, stored

https://doi.org/10.1021/acs.est.5c09148
Environ. Sci. Technol. XXXX, XXX, XXX−XXX

at −4 °C, and, upon return to the laboratory, OPE extraction was performed using solid-phase extraction (SPE). All the solid-phase samples, including PUFs, GFFs, quartz fiber filters, and sediment samples, were wrapped in tinfoil zip-lock bags and stored at −20 °C. Detailed sampling and extraction procedures are provided in Text S2. For microbial community analysis, 20 L of seawater was collected using sterile Niskin bottles mounted on a CTD rosette. Water samples were filtered through a sterile stainless-steel disc filter (Sartorius, Göttingen, Germany) fitted with a sterile 0.22 μm pore-size polycarbonate membrane (Φ142 mm; Millipore, Billerica, USA). The filtration apparatus was cleaned with 75% ethanol prior to use. After filtration, the membrane was folded, placed into a 50 mL enzyme-free cryovial (Corning, Beijing, China), flash-frozen in liquid nitrogen, and stored at −80 °C. The total storage time from sampling to DNA extraction was less than 50 days.

2.3. Extraction and Instrumental Analysis. Two deuterium-labeled OPEs, i.e., tributyl phosphate-d_{27} (TNBP-d_{27}) and triphenyl phosphate-d_{15} (TPHP-d_{15}), were used as analytical surrogates. The target OPEs in all aqueous samples were extracted via SPE, and Soxhlet extraction was used for extracting other solid-phase samples (Text S2).[6,29,30] OPEs were qualitatively and quantitatively analyzed using an Agilent gas chromatography−tandem mass spectrometry (GC−MS/MS) instrument, and details of the instrumental parameters and temperature program are presented in Table S2 and Text S2.

2.4. Quality Assurance and Quality Control. Air samples were collected on the windward side of the ship's foredeck to minimize background contamination. Possible contamination was monitored using field blanks, experimental blanks, program blanks, and repeated samples. Instrumental detection limits (IDLs) were established based on a signal-to-noise ratio obtained from three times the analyte in the minimum standard. OPE concentrations in all blank samples were below or comparable to the IDLs, and all samples were corrected using field blanks. Method detection limits (MDLs) were calculated by dividing the 3-fold IDLs by the volume or mass of the sample. The MDLs for surface seawater, bottom seawater, atmospheric, and sediment samples were 0.0005−0.0300 ng/L, 0.0038−0.2415 ng/L, 0.0002−0.0112 ng/m^3, and 0.0075−0.4831 ng/g, respectively. TNBP-d_{27} and TPHP-d_{15} were used to monitor sample recovery, which ranged from 88.4% to 117%. The relative standard deviations of measured OPE concentrations in the spike matrix ranged from 0.52% to 18.9%. The reported concentrations were not corrected for surrogate recovery on an individual basis but were adjusted for procedural contamination by subtracting the mean concentration measured in the procedural blanks from each sample.

2.5. Bioinformatic Processing of 16S rRNA Sequencing Data. The methods for DNA extraction and 16S rRNA sequencing are described in Text S4. Raw sequencing reads (~50,000 reads per sample) were initially processed using fastp v0.19.[31] Quality control included the removal of low-quality bases (Q-score < 20) and adapter sequences. All samples demonstrated exceptionally high sequencing quality, with Phred quality scores ($Q30$) ranging from 97.9% to 98.9%, well above the widely adopted threshold for high-quality data ($Q30$ > 90%). These metrics indicate a very low error rate, confirm high sequence reliability, and support the robustness of the data for downstream bioinformatic analyses. Next, filtered high-quality reads were imported into QIIME2 v2022.2[32] for comprehensive microbiome analysis. Sequence processing was performed using the DADA2 algorithm,[33] which implemented a three-step denoising pipeline involving (i) the modeling of errors originating during amplification and sequencing and the use of this model to correct random sequencing errors, (ii) the precise merging of paired-end reads, and (iii) the generation of a high-resolution amplicon sequence variant (ASV) table containing exact biological sequences with their corresponding abundance profiles for all samples. For taxonomic classification, the representative sequences from each ASV were aligned with the SILVA ribosomal RNA database (SILVA; release 138; https://www.arb-silva.de/) using a naive Bayes classifier. The classification process used a bootstrap confidence threshold of 0.7 to ensure taxonomic assignment reliability.[34] To maintain data integrity, chimeric sequences and nonmicrobial sequences (i.e., mitochondrial, chloroplast, and eukaryotic-derived reads) were systematically filtered from the data set. Using these stringent quality control measures, only high-confidence bacterial ASVs were retained for the subsequent ecological analyses.

2.6. Data Analysis. *2.6.1. Microbial Community Characterization and Statistical Analyses.* Phylogenetic reconstruction was conducted by performing the multiple sequence alignment of representative ASV sequences using MAFFT v7.2[35] with default parameters, followed by maximum-likelihood tree construction using IQ-TREE.[36] The microbial α-diversity was estimated using the inverse Simpson index, and the β-diversity was calculated using Bray−Curtis dissimilarities between samples based on the high-confidence ASV data set. All diversity metrics were computed using the vegan package (v2.7-1) in R. Significant differences in the α-diversity among groups were assessed using Kruskal−Wallis tests. To evaluate variations in community structures, permutational multivariate analysis of variance (PERMANOVA) was performed on Bray−Curtis dissimilarity matrices with 9999 permutations, and results were visualized using nonmetric multidimensional scaling (NMDS) ordination plots.

The genus-level community composition was analyzed using relative abundance data normalized by the total sum scaling. Correlations between environmental variables and community structures were determined using partial Mantel tests, and microbial compositional variation among samples and environmental dissimilarity matrices were calculated using Canberra distance matrices while controlling for the dissolved oxygen concentration as a covariate. Community assembly processes were quantitatively assessed using a null model approach[37] with 999 randomizations, incorporating phylogenetic (β-nearest taxon index, βNTI) and taxonomic (Raup−Crick index, RCbray) metrics. Ecological processes were categorized as follows: (1) homogeneous selection (βNTI < −2), (2) heterogeneous selection (βNTI > +2), (3) dispersal limitation (|βNTI| < 2 and RC_{bray} > 0.95), (4) homogeneous dispersal (|βNTI| < 2 and RC_{bray} < −0.95), and (5) drift (|βNTI| < 2 and |RC_{bray}| < 0.95).

Depth-stratified microbial biomarkers were identified using the linear discriminant analysis effect size (LEfSe),[38] with significant differences in relative abundances (p < 0.05) confirmed using Kruskal−Wallis H tests. The functional potential was predicted from 16S rRNA gene sequences using the Phylogenetic Investigation of Communities by Reconstruction of Unobserved States (PICRUSt2)[39] with KEGG and MetaCyc pathway databases.[40,41] The abundance of OPE-degrading enzymes was visualized via heatmap analysis using the R heatmap package.

https://doi.org/10.1021/acs.est.5c09148
Environ. Sci. Technol. XXXX, XXX, XXX−XXX

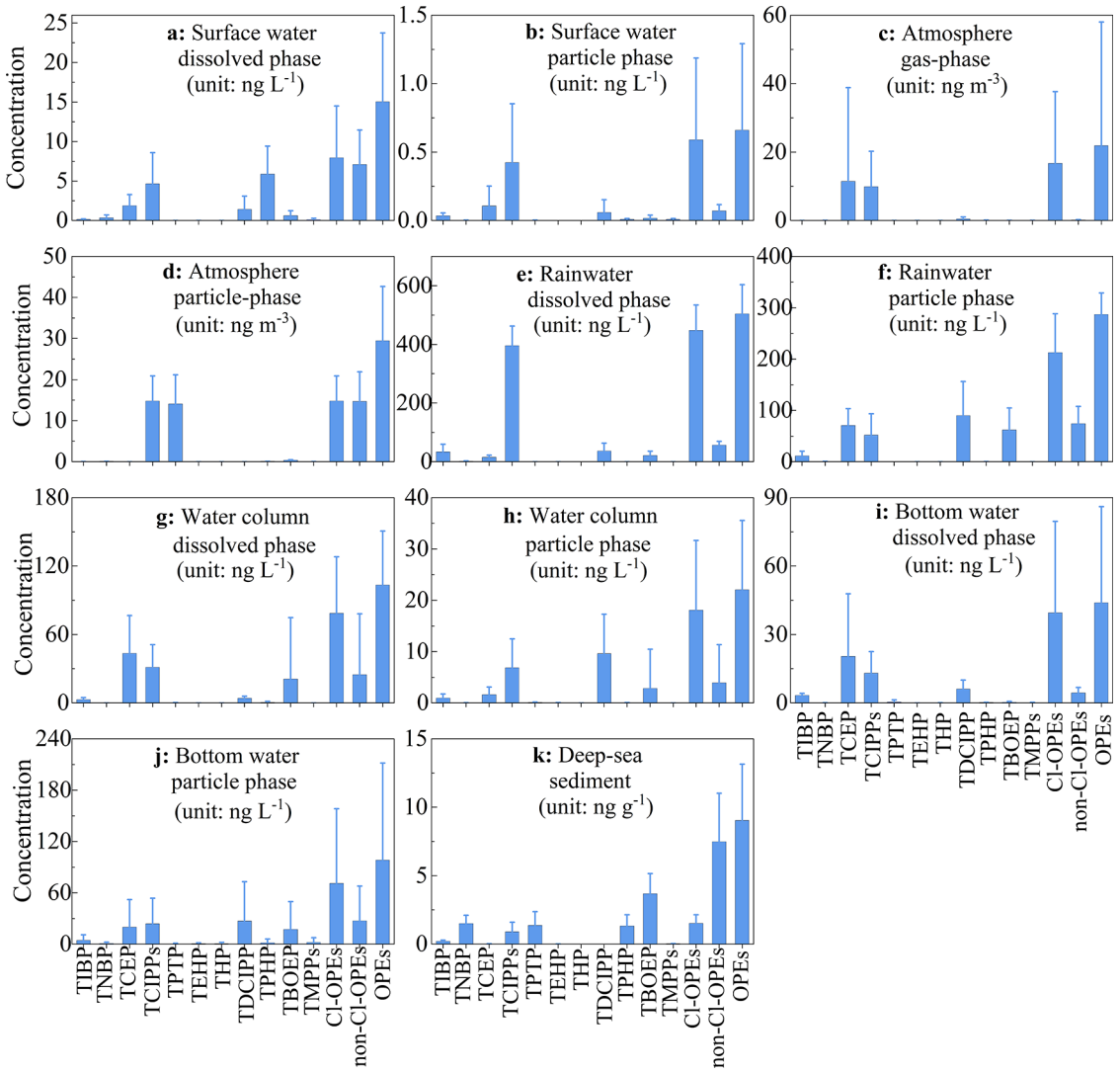

Figure 2. Organophosphate ester concentrations in different environmental media of the surface system (a–f) and deep-sea system (g–k) in the WSCS.

2.6.2. OPE Concentration Analysis. SPSS 26.0 was used for the statistical analysis of OPE concentrations. A student's *t*-test or a nonparametric test was used to ascertain the existence of differences in OPE concentrations between different groups. A *p*-value of <0.05 indicated a statistically significant result, and a *p*-value of <0.01 indicated a highly statistically significant result.

3. RESULTS AND DISCUSSION

3.1. Widespread Occurrence and Spatial Trends of OPEs in the WSCS. *3.1.1. Surface System.* Eleven target OPEs were simultaneously monitored in the gas and particle phases of the atmosphere, as well as in the dissolved and particle phases of surface seawater and rainwater in the WSCS. The majority of OPEs were detected across these environmental media. All 11 OPEs were detected in the atmospheric environment, with 11 in the gas phase and 9 in the particle phase. In surface seawater, nine OPEs were detected, with only tri(2-ethylhexyl) phosphate (TEHP) and trihexyl phosphate (THP) not detected. These results indicate that OPE contamination was pervasive within the WSCS surface system.

3.1.2. Atmosphere. The total concentrations of the 11 target OPEs ($\sum_{11}$OPEs) in the gas phase (21.9 ± 36.2 ng/m^3) were slightly lower than those in the particle phase (29.5 ± 13.2 ng/m^3) (Figures S2d and S3c). The total concentration of the eight non-Cl-OPEs ($\sum_{8}$non-Cl-OPEs) was approximately 40 times higher in the particle phase (48.6% ± 4.41%) than in the gas phase (1.39% ± 1.27%). For the 11 OPEs in the gas phase, the total concentration of the three chlorinated OPEs ($\sum_{3}$Cl-OPEs, 16.7 ± 21.0 ng/m^3) was significantly higher than that of the $\sum_{8}$non-Cl-OPEs (0.12 ± 0.13 ng/m^3) (nonparametric test, p < 0.01). In the particle phase, $\sum_{3}$Cl-OPEs (14.8 ± 6.12 ng/m^3) and $\sum_{8}$non-Cl-OPEs (14.7 ± 7.19 ng/m^3) were comparable. The atmospheric concentrations of OPEs observed in this study were higher than those reported in the Southern Ocean,[42] the Northern Pacific and Indian Oceans,[43] and the Atlantic, Pacific Oceans.[44]

3.1.3. Rainwater. $\sum_{11}$OPEs in the dissolved phase (505 ± 98.7 ng/L) was significantly higher than that in particle phase (287 ± 41.7 ng/L; *t*-test, p < 0.01; Figure 2e,f). $\sum_{3}$Cl-OPEs (dissolved phase: 448 ± 86.0 ng/L, particle phase: 213 ± 75.4 ng/L) was significantly higher than $\sum_{8}$non-Cl-OPEs (dissolved phase: 56.7 ± 12.8 ng/L, particle phase: 74.2 ± 33.6 ng/L). These concentrations were slightly higher than those in the intertropical convergence zone (ITCZ).[14]

https://doi.org/10.1021/acs.est.5c09148
Environ. Sci. Technol. XXXX, XXX, XXX−XXX

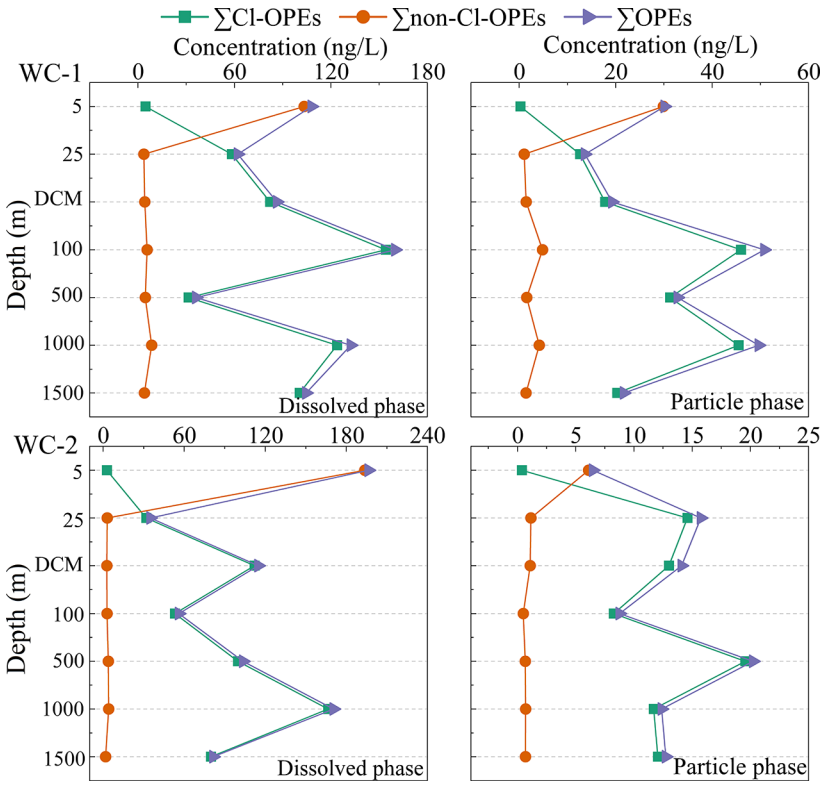

Figure 3. Variations in OPE concentrations in the two water columns (WC-1 is in the open water, deep chlorophyll maximum (DCM) = 75 m; WC-2 is close to the Zhongsha Atoll, DCM = 95 m) in the WSCS.

3.1.4. Surface Seawater. $\sum_{11}$OPEs in surface seawater were notably lower than those in rainwater. In the dissolved phase, $\sum_{11}$OPEs (15.0 ± 8.70 ng/L) were much higher than in the particle phase (0.66 ± 0.63 ng/L; *t*-test, $p < 0.01$; Figure 2a,b). Among these, $\sum_{3}$Cl-OPEs (7.95 ± 6.55 ng/L) and $\sum_{8}$non-Cl-OPEs (7.10 ± 4.37 ng/L) were comparable in the dissolved phase, whereas in the particle phase, $\sum_{3}$Cl-OPEs (0.59 ± 0.60 ng/L) were significantly higher than $\sum_{8}$non-Cl-OPEs (0.07 ± 0.05 ng/L). The OPE concentrations obtained were lower than those reported in the South Pacific,[45] the Atlantic Ocean,[14] Northwest Pacific and Arctic Oceans,[46] but close to those in the Southern Ocean.[5,14]

3.1.5. Deep-Sea System. All target OPEs were detected to varying extents in the dissolved and particle phases of seawater, with detection rates of 45.5−100% and 63.6−100%, respectively. Eight OPEs were detected in all deep-sea sediment samples, with a detection rate of 100%, while TEHP, THP, and tri(dichloroisopropyl) phosphate (TDCIPPs) were not detected.

3.1.6. Water Column Depth Profiles in Different Sea Areas. $\sum_{11}$OPEs in the dissolved phase (95.3 ± 42.6 ng/L) were significantly higher than in the particle phase (22.7 ± 13.7 ng/L; *t*-test, $p < 0.01$), and $\sum_{3}$Cl-OPEs were significantly higher than $\sum_{8}$non-Cl-OPEs in both the dissolved and particle phases (Figure 3). These concentrations were comparable to those reported in the Mariana Trench,[10] the Atlantic Ocean, and the Southern Ocean.[14]

In the open sea area (WC-1), $\sum_{11}$OPEs exhibited a consistent trend of change in particle and dissolved phases, i.e., $\sum_{11}$OPEs continuously increased from the surface to a depth of 100 m, suddenly decreased at a depth of 500 m, increased at a depth of 1000 m, and finally decreased at a depth of 1500 m. The highest $\sum_{11}$OPEs in the particle (50.8 ng/L) and dissolved (160 ng/L) phases were observed at a depth of 100 m (Figure 3).

In the sea area near the coral reef (WC-2), the observed trends in $\sum_{11}$OPEs exhibited notable differences between the dissolved and particle phases. The highest $\sum_{11}$OPEs in the dissolved phase was observed at the surface layer, while the highest $\sum_{11}$OPEs in the particle phase was observed at a depth of 500 m. From the surface to the subsurface layer (25 m), $\sum_{11}$OPEs in the dissolved phase decreased sharply and then significantly increased in the deep chlorophyll maximum (DCM) layer (Figure 3). This surface enrichment, accompanied by subsurface depletion, was attributed to the sinking and adsorption of PM, a process that is exacerbated by the nearby cold eddies. Conversely, the increased OPE concentration in the DCM layer was attributed to the increase in the phytoplankton biomass, which in turn affects the sinking of PM. Potential microbial activities may also be involved in OPE degradation. In the particle phase, $\sum_{11}$OPEs were highest at 25 m and gradually decreased with increasing depth, with the lowest concentrations observed at 100 m. Across all depth profiles from 100 to 1500 m, $\sum_{11}$OPEs first increased and then decreased; the difference was that the highest $\sum_{11}$OPEs in the dissolved phase (171 ng/L) occurred at 1000 m, whereas the highest $\sum_{11}$OPEs in the particle phase (20.2 ng/L) occurred at 500 m (Figure 3).

As mentioned above, the photochemical degradation process significantly reduced the concentration of Cl-OPEs in surface seawater compared to other layers in the vertical profile, and microbial activity in the subsurface layer of the ocean may dominate the degradation of non-Cl-OPEs in the vertical profile. Still, the distribution of OPEs in WC-1 and WC-2 water columns differed. Coral reef regions have a higher biodiversity and primary productivity, increasing PM concentration in the surrounding seawater. In WC-2, a high concentration of

https://doi.org/10.1021/acs.est.5c09148
Environ. Sci. Technol. XXXX, XXX, XXX−XXX

$\sum_{11}$OPEs in the dissolved phase may adsorb onto PM or coral mucus during the uninterrupted sinking process of PM. After obtaining the highest $\sum_{11}$OPEs in the particle phase at a 500 m depth, the sinking and dissolution of mucus and PM led to the re-entry of particle-phase OPEs into the dissolved phase of the water column. This process may have substantially increased $\sum_{11}$OPEs in the dissolved phase at a 1000 m depth. Additionally, the process of resuspension, induced by deep-sea currents, may have further increased the concentration of dissolved OPEs. Furthermore, except for surface seawaters, $\sum_{3}$Cl-OPEs was higher than $\sum_{8}$non-Cl-OPEs in all depth profiles. The exceptionally high value of $\sum_{8}$non-Cl-OPEs in surface seawater contributed to the high values of $\sum_{11}$OPEs (Figure 3).

3.1.7. Bottom Seawater. $\sum_{11}$OPEs in the particle phase (38.0 ± 49.1 ng/L) were comparable to those in the dissolved phase (44.0 ± 42.2 ng/L; *t*-test, $p < 0.01$), and $\sum_{3}$Cl-OPEs were significantly higher than $\sum_{8}$non-Cl-OPEs in both the dissolved and particle phases (Figure 2i,j). These concentrations were higher than those reported in the Atlantic and Southern Oceans,[14] but were comparable to those in the Mariana Trench.[10]

3.1.8. Deep-Sea Sediment. $\sum_{11}$OPEs ranged from 2.70 to 15.6 ng/g (8.13 ± 3.13 ng/g), and $\sum_{8}$non-Cl-OPEs (8.13 ± 3.63 ng/g) were significantly higher than $\sum_{3}$Cl-OPEs (0.92 ± 0.71 ng/g; Figure 2k). These OPE concentrations were higher than those reported in the Arctic Ocean,[47,48] but lower than those in the Eastern Indian Ocean,[49] the Mariana Trench,[10] and the Bohai Sea and East China Sea.[50]

3.1.9. Spatial Distribution of OPEs. 3.1.9.1. Spatial Differences and Influencing Factors in the Atmosphere. $\sum_{11}$OPEs in the atmospheric environment exhibited regional differences in the entire survey area, with higher values in the South and lower values in the North. High-$\sum_{11}$OPE regions were detected near the Indochina Peninsula and Zhongsha Islands (Figure 1b2). The southwest monsoon drives the transport of terrigenous pollution sources in the Indochina Peninsula, negatively affecting the SCS ecosystem.[51−53] The 72 h backward air mass trajectory showed the significant impact of the southwest monsoon on the SCS ecosystem during the sampling period (Figure S1). Terrestrial sources of pollution, such as electronics dismantling and waste incineration,[21,54] could continue releasing OPEs, which are transported to the SCS via the LRT of the air mass driven by the summer monsoon (Figure S2b). Additionally, the high-concentration zone of OPEs near the Zhongsha Islands was precisely located along the main shipping route in the SCS,[55] indicating that ship navigation could have been responsible for releasing OPE-related pollutants into the atmospheric environment.

The occurrence of OPEs in the atmosphere was influenced by monsoon and diurnal variations in the WSCS. Atmospheric OPE concentrations were markedly higher during the southwest monsoon than during the southeast monsoon, particularly in the gas phase (Figure S3d). The southwest monsoon likely contributed predominantly to the input of non-Cl-OPEs, whereas the southeast monsoon predominantly contributed to Cl-OPEs. Maritime human activities, including fishing, offshore oil drilling, and shipping, may have contributed to OPE inputs into the atmosphere (Figures S3a and 2d). The global electronic component manufacturing plant and supply base on Luzon Island was also responsible for transporting pollutants into the WSCS atmosphere via air masses (Figure 1b2). Diurnal variations influenced atmospheric OPE concentrations, with particle-phase OPE concentrations higher during daylight and gas-phase OPE concentrations higher at night (Figures S3e and 2h). This discrepancy was attributed to the higher photodegradation capacity of Cl-OPEs in the gas phase compared to the particle phase.

3.1.9.2. Gas/Particle Partitioning. Gas/particle partitioning determines the environmental fate of SVOCs, especially their LRT and migration in the atmosphere, and affects the bioavailability of SVOCs.[56,57] A comparison between the estimated K_P values of different models and the field values is shown in Figure S4. The comparison shows that the K_P values of the target OPEs predicted using the Harner−Bidleman adsorption model were close to the actual values (Figure S4e,f). The Junge−Pankow model fitted the correlation between the temperature-corrected subcooled liquid vapor pressure (P_L^0) and calculated values of K_P, but the slope was significantly different from the theoretical value at equilibrium (Figure S4a,b). By contrast, the K_P values for all 11 OPEs predicted using the $K_{soot\text{-}air}$ double-adsorption model were much lower than the actual values (Figure S4c,d). Furthermore, although the steady-state model predicted K_P values for some OPEs that were close to the actual values, there was a significant deviation between the predicted values and actual values for five OPEs (Figure S4g,h). New pollution sources, LRT, physical and chemical properties of OPEs, field sampling, air temperature, and activity coefficients affect the K_P of SVOCs, leading to the deviation between the actual and simulated values.[16,57,58]

3.1.9.3. Spatial Differences and Influencing Factors in the Surface Seawater. The high-value area of $\sum_{11}$OPEs covered the Hainan Island and Xisha Island (Figure 1b1), which experience frequent human activities. High concentrations of OPEs (28.0−40.5 ng/L) were detected in the northeastern region of the Hainan Island (W2 and W3). Of these, Cl-OPEs constituted 68.5−72.7% of the total, and the concentration of tris(2-carboxyethyl) phosphine (TCEPs) and tris(2-chloroisopropyl) phosphates (TCIPPs) reached their zenith, indicating that industrial discharges in the northeastern region of the Hainan Island (i.e., wastewater discharge and shipbuilding and maintenance) significantly impacted the spatial distribution of OPEs. Moreover, OPEs unintentionally generated during industrial activities in southern China entered the SCS via Pearl River runoff. There were well-established electronics dismantling and recycling industry chains in Qingyuan and Shantou, Guangdong Province, which may aggravate the pollution of OPEs in the Pearl River and SCS.[11,59] However, the current-driven transport and dispersion of OPEs in the northern SCS had a minimal impact on the distribution characteristics of OPEs in the surface water of the study area, as evidenced by the currents in the SCS during the sampling period (Figure S2a). Furthermore, the western boundary current (WBC), a primary driver of the northward migration and dispersion of water masses from the Mekong River and terrigenous pollution sources in the Central South Peninsula, could exacerbate OPE contamination (Figure S2a). Continuous runoff inputs from the Mekong River have exacerbated the pollution from dissolved black carbon, polycyclic aromatic hydrocarbons, and other organic matter in the WSCS.[17,52] Unfortunately, OPE pollution may pose a significant ecological threat to the numerous coral reefs in Hainan and Xisha Islands and increase the risk to human health through transfer along the food chain.[6,60] The target OPEs were significantly correlated in each environmental medium of the deep-sea and surface systems

https://doi.org/10.1021/acs.est.5c09148
Environ. Sci. Technol. XXXX, XXX, XXX−XXX

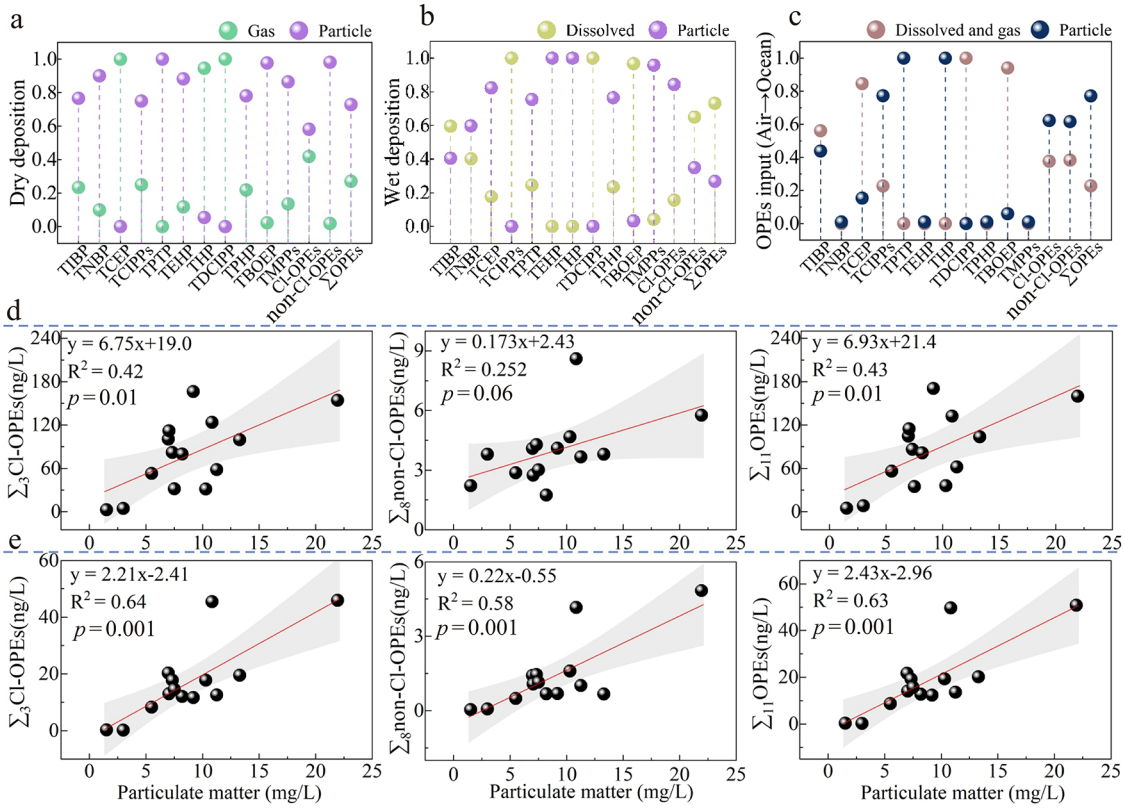

Figure 4. Contribution rates of different phases during OPE migration from the atmosphere to the ocean: (a) dry deposition, (b) wet deposition, and (c) total input flux. Correlation between particulate matter and OPE concentrations in the (d) dissolved and (e) particle phases of the water column.

(Figure S5), indicating that the OPEs in each environmental medium of the WSCS had similar potential sources.

3.2. Atmospheric Deposition as a Dominant Input Pathway. *3.2.1. Air–Water Exchange.* A modified two-layer model was used to calculate the air–water exchange flux of OPEs (Text S6).[61−63] The net flux range of the studied $\sum_{11}$OPEs was from 22.8 to 3012 ng/m^2/d, with an average value of 783 ± 810 ng/m^2/d, indicating that OPEs were evaporated from the ocean to the atmosphere during sampling period. Among them, the net flux of $\sum_3$Cl-OPEs (435 ± 564 ng/m^2/d) was higher than that of $\sum_8$non-Cl-OPEs (334 ± 314 ng/m^2/d), and TCIPPs and TPHPs were the dominant contributors to these two types of fluxes, respectively (Figure 4a).

3.2.2. Atmosphere Deposition. Atmospheric deposition has been successfully used to investigate the vertical migration of SVOCs (Text S6).[21,64] The calculated dry deposition fluxes ranged from 6161 to 58,165 ng/m^2/d (17,463 ± 9734 ng/m^2/d); the dry deposition fluxes of $\sum_3$Cl-OPEs (11,085 ± 8238 ng/m^2/d) were considerably higher than those of $\sum_8$non-Cl-OPEs (6379 ± 3105 ng/m^2/d; *t*-test, $p < 0.01$). The dry deposition fluxes of $\sum_{11}$OPEs in the particle phase (12,734 ± 5704 ng/m^2/d) were significantly higher than those in the gas phase (4729 ± 2592 ng/m^2/d; *t*-test, $p < 0.01$; Figure S7b,c). Some studies have demonstrated that wind speed, humidity, particle size, and physicochemical properties of compounds can affect dry deposition rates.[65,66] The wet deposition fluxes of OPEs ranged from 3521 to 9307 ng/m^2/d (6602 ± 2893 ng/m^2/d), and $\sum_8$non-Cl-OPEs were predominant (92.1% ± 1.74%; Figure S7d,e). Unlike dry deposition, wet deposition fluxes of $\sum_{11}$OPEs in the dissolved phase (4834 ± 2256 ng/m^2/d) were significantly higher than those in the particle phase (1768 ± 825 ng/m^2/d; *t*-test, $p < 0.01$; Figure S7b,c).

These results imply that PM plays an important role in the input of marine OPEs via atmospheric deposition and exerts a substantial influence on their vertical transport. For dry deposition, more than 27.1% of OPEs and 41.6% of Cl-OPEs deposited from the atmosphere into the ocean were attributable to PM (Figure 4a). Similarly, PM accounted for more than 27.0% of OPEs and 84.4% of Cl-OPEs transported vertically during wet deposition (Figure 4b).

3.2.3. Deep-Sea Sediment-Water Diffusion. The absorption/desorption characteristics of deep-sea sediments for OPEs were explored according to the procedures reported in our previous studies (Text S8).[17,20,67] As shown in Figure S8b, deep-sea sediments showed potential adsorption tendencies for the majority of OPEs in bottom seawater ($\log f < -0.12$), indicating that deep-sea sediments are potential sinks for OPEs in the water column of the WSCS. Moreover, the difference between the experimental K_{OC} and average field K_{OC} increased with increasing experimental K_{OC}, indicating that the adsorption capacity of sediments for OPEs increased with increasing KOC of the OPEs. The calculated log K_{OC} of OPEs was significantly correlated with their log K_{OW} ($R^2 = 0.65$, $p < 0.01$), demonstrating that the partitioning of OPEs between deep-sea sediment-water systems was significantly influenced by hydrophobic interactions (Figure S8a). The chemical structure of OPEs was closely related to the calculated log K_{OC}, which increased with increasing number of carbon atoms for non-Cl-OPEs and with increasing number of chlorine atoms for Cl-OPEs.[68]

In summary, the net atmospheric transport (20,460−27,085 ng/m^2/d) to the marine environment was the dominant process transporting OPEs to the WSCS, primarily via atmospheric deposition (Figure S7f). OPEs, especially chlorinated com-

https://doi.org/10.1021/acs.est.5c09148
Environ. Sci. Technol. XXXX, XXX, XXX−XXX

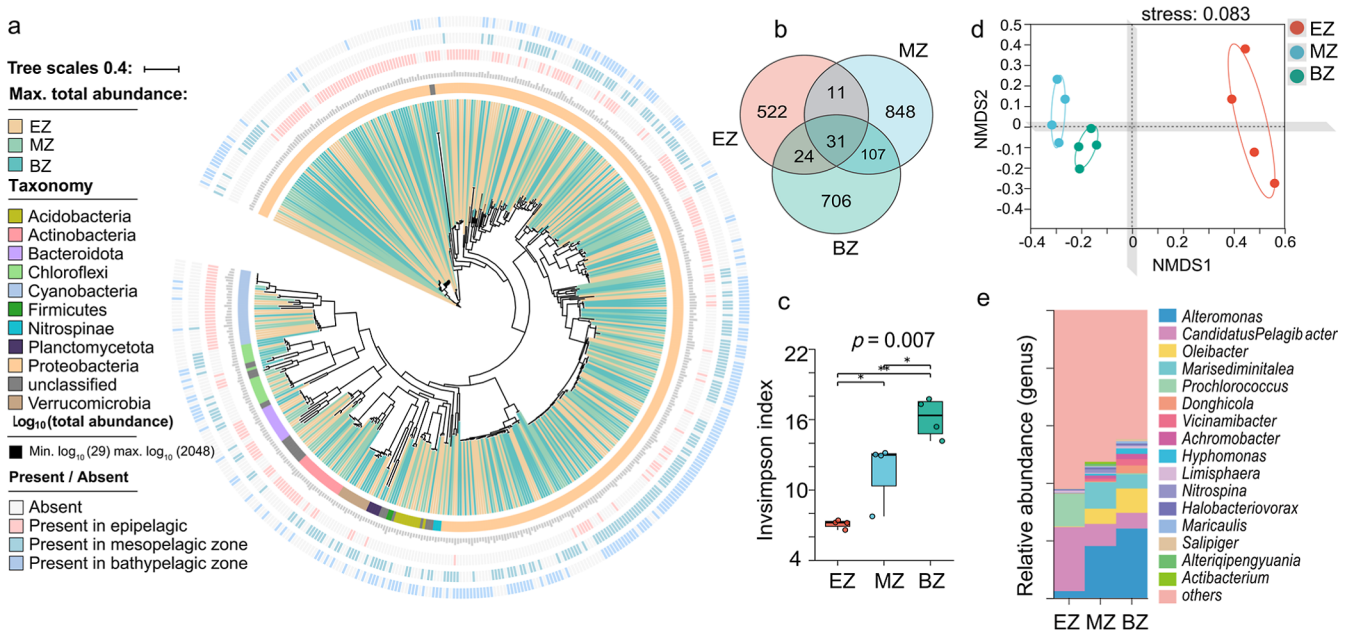

Figure 5. Vertical stratification characteristics of the bacterial diversity and community structure in seawater of the WSCS. (a) Phylum-level phylogenetic tree of the top 500 abundant ASVs (highlighting 10 dominant bacterial phyla). (b) Shared and unique ASVs among three zones (i.e., EZ, MZ, and BZ). (c) Taxonomic diversity (InvSimpson index) in three zones (n = 12; Kruskal−Wallis H test, *p < 0.05, **p < 0.01). (d) NMDS based on Bray−Curtis dissimilarities (PERMANOVA by Adonis, n = 12). (e) Relative abundance (%) of the top 16 bacteria in three zones.

pounds such as TCIPPs and TCEP, have high KP values and readily adsorb onto atmospheric PM. This results in high concentrations of OPEs in the atmospheric particle phase, and particulate-bound OPEs are more likely to enter the ocean via dry or wet deposition. Air−water exchange, however, depends on diffusion processes at the sea−air interface, and most OPEs have low Henry's constants, leading to weak volatilization from the sea surface to the atmosphere. Consequently, net atmospheric deposition was identified as the predominant pathway for OPEs entering the WSCS, exceeding the volatilization flux by orders of magnitude. Atmospheric deposition dominated the vertical transport of atmospheric OPEs, influencing their biogeochemical cycling and exacerbating ecological pressure on marine ecosystems, particularly coral reefs. Importantly, PM contributed 65.3−98.4% (58.6% ± 16.5%) of the total input of atmospheric OPEs into the ocean (Figure 4c), while deep-sea sediments were identified as a potentially significant sink for OPEs in the deep-sea environment (Figure S8).

3.3. Vertical Transport of OPEs and Biogeochemical Cycles. As shown in Figure 3, $\sum_{11}$OPEs in the two water columns of the WSCS exhibited significant differences. However, when the water column was divided into an epipelagic zone (EZ; 0−100 m), a mesopelagic zone (MZ; 100−500 m), and a bathypelagic zone (BZ; 1000−1500 m), OPEs exhibited a pronounced depletion in the surface layer and an enrichment in the deep sea. This distribution pattern was consistent in the dissolved and particle phases of seawater. The following order of $\sum_{11}$OPEs was observed in the dissolved and particle phases: BZ (106 ± 26.4 and 72.7 ± 29.2) > MZ (80.2 ± 17.5; 52.1 ± 3.45) > EZ (49.9 ± 31.6 and 31.6 ± 25.4; Figures S3 and S6). This pronounced heterogeneity may reflect the general pattern of the OPE distribution in the vertical profile of seawater in the WSCS.

3.3.1. Vertical Transport Driven by Particulate Matter. Material and energy transport in the ocean's vertical profile is linked to MBLPs, which play a crucial role in nutrient cycling and carbon sequestration in the deep sea.[69] The vertical transport processes of OPEs in the ocean affect their biogeochemical cycling processes in the global ocean.[49] OPEs in seawater depth profiles originate from the surface environment of oceans and combine with PM, phytoplankton, and biological detritus via biogeochemical cycling to sink to the deep sea under the action of MBLPs. Numerous studies have confirmed that organic pollution in the deep-sea environment originates from the surface system.[10,14,17,70] A clear correlation exists between OPEs in various environmental media in the surface and deep sea in the WSCS (Figure S5). As shown in Figure 4d,e, a notable positive correlation exists between OPE concentrations and PM in the WSCS vertical profile. The sinking of PM plays a pivotal role in shaping the distribution of OPEs along the depth profile, thereby influencing their vertical transport. Ocean snow, formed by the sinking of phytoplanktonic organic matter, organic particles, dead organisms, and feces, transports nutrients to the deep sea and also adsorbs and transports OPEs from surface waters to deeper ocean layers, thereby altering the concentration and composition of OPEs at different depths (Figure 4d,e). The interaction between sinking particles and OPEs may also influence the bioavailability of OPEs and their potential impacts on marine ecosystems throughout the water column. Therefore, PM in seawater drives the distributional characteristics of OPEs in the WSCS depth profile and also influences the environmental behavior of OPEs in the water column. PM plays an important role in the vertical transport of marine surface OPEs to the deep-sea environment, which most likely also influences the biogeochemical cycling of OPEs in the deep-sea environment.

3.3.2. Microbial Community Response and the Biological Pump of OPEs. The high-throughput 16S rRNA gene sequencing analysis of seawater samples from the EZ, MZ, and BZ showed distinct microbial community structures in these zones. Phylogenetic analysis of the top 500 most abundant ASVs demonstrated clear phylum-level clustering, with extremely low

https://doi.org/10.1021/acs.est.5c09148
Environ. Sci. Technol. XXXX, XXX, XXX−XXX

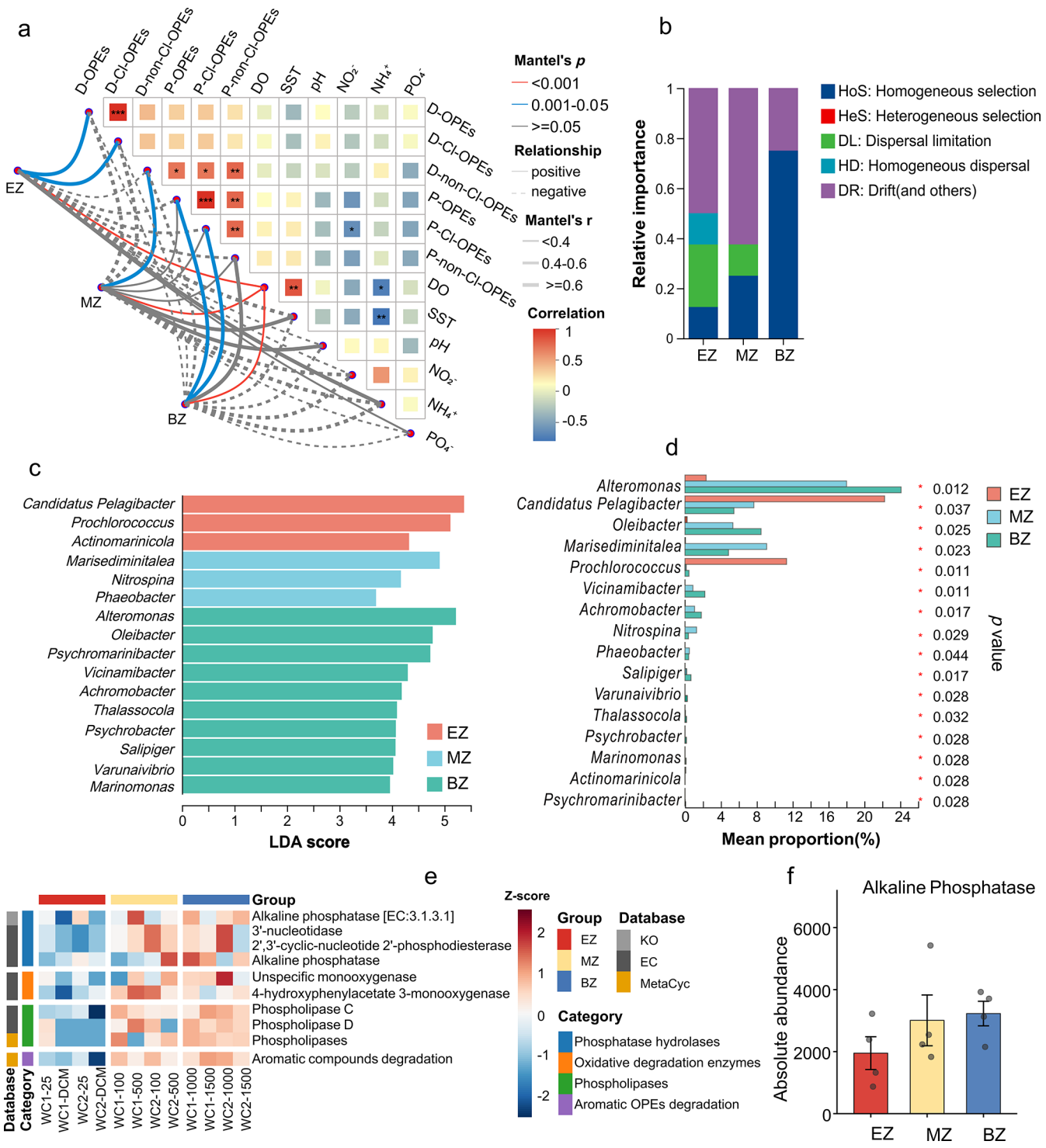

Figure 6. Microbial community assembly and degradation mechanisms driving the vertical partitioning of OPEs in the WSCS. (a) Associations between microbial community structure (based on Canberra distance) and environmental variables (based on Canberra distance) analyzed using partial Mantel tests. Partial Mantel's p values are indicated by edge color (solid and dashed lines represent positive and negative correlations, respectively), while partial Mantel's r values are represented by edge width. Statistical significance is denoted by edge color. Pairwise correlations between environmental variables are depicted using a color gradient reflecting Spearman's correlation coefficients, with statistical significance denoted as follows: $^{*}p < 0.05$, $^{**}p < 0.01$, and $^{***}p < 0.001$. (b) Relative contribution of each ecological process driving microbial community assembly within different water layers, based on null model analysis. (c) Identification of biomarkers in different zones by LEfSe. (d) Relative abundances of significantly differentiated biomarkers (Kruskal–Wallis H test, $p < 0.05$) in the EZ, MZ, and BZ. (e) Heatmap of the relative abundance of key OPE-degrading enzyme genes in different zones. (f) Alkaline phosphatase abundance increases with increasing water depth.

taxonomic overlap between the different zones (Figure 5a). These ASVs were predominantly distributed among the following phyla: Acidobacteria, Actinobacteria, Bacteroidota, Chloroflexi, Cyanobacteria, Firmicutes, Nitrospinae, Planctomycetota, Proteobacteria, unclassified taxa, and Verrucomicrobia (Figure 5a). Notably, only 31 ASVs (1.38%) were common

https://doi.org/10.1021/acs.est.5c09148
Environ. Sci. Technol. XXXX, XXX, XXX−XXX

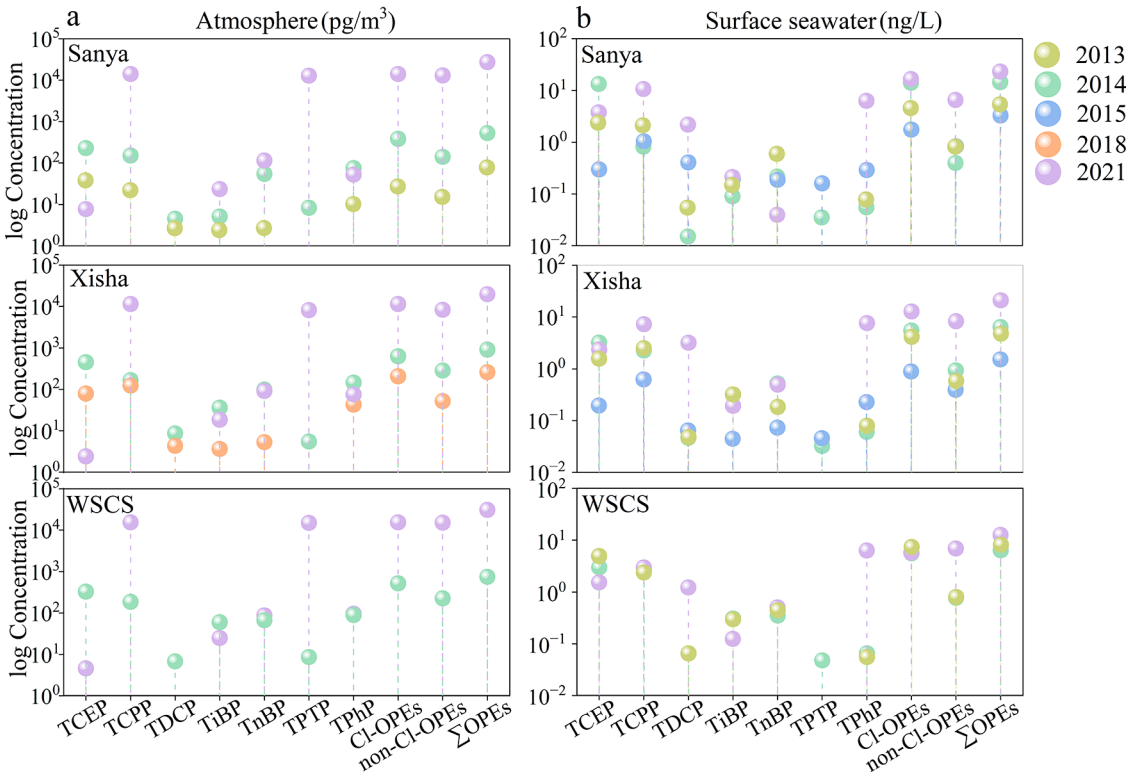

Figure 7. (a,b) Characteristics of interannual variability of OPE concentration levels in the SCS (atmosphere here represents only the atmospheric particle phase).

in all the three zones (Figure 5b). The MZ and BZ exhibited a higher community similarity (138 ASVs) but shared only 42−55 ASVs with the EZ. Furthermore, 522, 848, and 706 unique ASVs were detected in the EZ, MZ, and BZ, respectively, further corroborating the distinct community structures of these three zones (Figure 5b). The microbial α-diversity analysis (InvSimpson index) exhibited a significant increasing trend with depth (Kruskal−Wallis test, $p < 0.01$), following the order of BZ > MZ > EZ (Figure 5c). NMDS ordination based on Bray−Curtis dissimilarities (stress = 0.08) confirmed vertical stratification (PERMANOVA; $R^2 = 0.64$, $p = 0.001$), with distinct clustering of communities by zones (Figure 5d). At the genus level, the relative abundance of Alteromonas increased with increasing water depth (EZ = 2.36%, MZ = 18.0%, BZ = 24.1%), indicating the potential niche-specific adaptations to OPE-rich deep-sea environments. By contrast, the relative abundance of Pelagibacter decreased with increasing water depth (EZ = 22.3%, MZ = 7.68%, BZ = 5.46%), reflecting its reduced competitive fitness in deeper, more polluted seawater (Figure 5e).

Partial Mantel tests demonstrated a significant correlation between microbial community composition and OPE concentrations (Figure 6a). Dissolved OPEs (D-OPEs) and dissolved chlorinated OPEs (D-Cl-OPEs) exhibited significant correlations with the EZ microbial community structure, whereas dissolved non-Cl-OPEs (D-non-Cl-OPEs) showed stronger correlations with the MZ microbial community structure. Notably, particle-associated OPEs in the BZ were predominantly linked to the BZ community structure, indicating that microbial niche partitioning was the primary driver of the vertical stratification of OPEs (Figure 6a).

Distinct assembly mechanisms governed microbial communities in different zones (Figure 6b). In the EZ, drift (DR) and dispersal limitation were the dominant forces. In the MZ, the community assembly was jointly regulated by DR and homogeneous selection (HoS). In the BZ, the selective pressure of HoS significantly increased, collaborating with DR to mold the community structure (Figure 6b). These shifts in assembly mechanisms provided a foundation for the microbial degradation of OPEs.

LEfSe analysis further elucidated the microbial degradation mechanisms. The seawater in the EZ was dominated by typical oligotrophic microorganisms, while that in the MZ was enriched with bacterial genera such as *Phaeobacter* with potential for OPE degradation.[71,72] The seawater in the BZ was significantly enriched with highly efficient OPE-degrading bacteria, including *Alteromonas* and *Marinomonas*,[15,72] accompanied by the colonization of various piezophilic bacteria (Figure 6c). Kruskal−Wallis H tests confirmed significant differences ($p < 0.05$) in the relative abundances of these biomarkers in the three zones, indicating that the concentration gradient of OPEs and the vertical profile drive the niche differentiation of microbial functional communities (Figure 6d). These degrading bacteria regulated the concentration distribution of OPEs in the MZ and BZ via the MBLP effect. The microbial degradation of OPEs was mediated by phosphoester hydrolase (including alkaline phosphatase and phosphodiesterase),[73] oxidative degradation enzymes (e.g., oxygenases), phospholipase, and enzymes involved in the degradation of aromatic OPEs.[74] PICRUSt2-based functional inference elucidated the molecular mechanisms underlying OPE biodegradation. The abundance of key enzymes involved in OPE degradation, predicted using different databases, such as KEGG Orthology (KO), enzyme commission (EC) number, and MetaCyc, increased significantly in the MZ and BZ (Figure 6e). Notably, the alkaline phosphatase abundance increased with increasing water depth (EZ < MZ <

https://doi.org/10.1021/acs.est.5c09148
Environ. Sci. Technol. XXXX, XXX, XXX−XXX

BZ; Figure 6f), in agreement with the accumulation of OPEs in the MZ and BZ. This finding confirms that deep-sea microbial communities adapt to the high-OPEs environment by upregulating phosphoester hydrolase, enabling the efficient degradation of OPEs and regulating their vertical distribution.

In summary, we have systematically revealed the significant impact of deep-sea microbial activity on the distribution patterns of OPEs from the perspectives of microbial community assembly mechanisms and functional adaptive evolution. Concentration differences in OPEs and vertical profiles shape distinct marine microbial community structures, and these microbial communities drive the degradation of OPEs in the ocean via microbial activities such as ecological niche differentiation and significant upregulation of the relative abundance of key degrading taxa (e.g., *Phaeobacter*, *Alteromonas*, and *Marinomonas*) and enhanced activity of OPE-degrading enzymes (e.g., alkaline phosphatase). These phenomena are indicative of the significant ecological role of microbial communities in driving the biogeochemical cycling of OPEs in the marine environment via multidimensional adaptive strategies.

Consequently, in addition to the focus on the physical migration processes of PM in the ocean, the regulatory role of microbial activity on the biogeochemical cycling of OPEs in the ocean is equally important. The vertical distribution of OPEs in the ocean is influenced by a combination of physical−chemical processes (e.g., PM sinking) and biological processes (e.g., marine microbial activity). These processes collectively determine the concentration levels and distribution patterns of OPEs in the ocean, thereby impacting the biogeochemical cycling of OPEs in marine ecosystems.

3.4. OPE Pollution Trends and Potential Impacts. The analytical results and existing studies reveal that the pollution of OPEs in the SCS shows an increasing trend.[28,75−78] The pollution levels of OPEs in the atmosphere increased significantly (Figure 7a). Compared to earlier reports on the concentration of seven OPEs ($\sum_7$OPEs) in the atmosphere,[28,76,77] $\sum_7$OPEs in the Hainan Island increased from 77.9 ± 26.0 pg/m^3 in 2013 to 524 ± 330 pg/m^3 in 2014 and then to the current level of 13,040 ± 7191 pg/m^3. $\sum_7$OPEs in the Xisha Islands and WSCS increased from 912 ± 469 pg/m^3 and 730 ± 244 pg/m^3 in 2014 to 8501 ± 2576 pg/m^3 and 15,211 ± 8758 pg/m^3, respectively, during this survey.

The pollution levels of OPEs in the surface seawater of the SCS also showed a general increasing trend (Figure 7b). According to these results and existing reports on $\sum_7$OPEs in surface seawater in the SCS,[28,75,78] $\sum_7$OPEs in the Hainan and Xisha islands increased from 5.38 ± 2.83 ng/L and 4.73 ± 2.14 ng/L in 2013 to 14.5 ± 9.97 ng/L and 6.38 ± 2.12 ng/L in 2014, respectively, and even though there was a slight decrease in 2015, $\sum_7$OPEs have increased to 22.7 ± 10.4 ng/L and 21.1 ± 3.48 ng/L during the sampling period. In the WSCS, there was a slight decrease in 2014 (6.30 ± 2.55 ng/L) compared to 2013 (8.31 ± 5.74 ng/L), but the contamination level was significantly higher during the sampling period (12.7 ± 6.28 ng/L).

The non-Cl-OPE concentration increased at a higher rate than the Cl-OPEs, potentially owing to increased human activities such as paint and coating use as well as the growth of plastics and electronics industries.[79] The presence of long-term plastic waste in the SCS may also result in OPE release under the influence of ultraviolet rays or microorganisms. Furthermore, the rapid development of the electronics manufacturing industry in China (Guangdong, Fujian) and Vietnam have led to the continuous migration of OPEs in electronic components to long distances into the SCS via runoff and atmospheric transport. Concurrently, increase in maritime trade and use of SCS shipping lanes significantly raises the likelihood of antifouling paint wear and hydraulic oil leaks entering the ocean, thereby exacerbating OPE pollution. This could exert greater ecological pressure on marine ecosystems (e.g., coral reefs) in the SCS and influence deep-sea ecosystems through coupled physical, chemical, and biological processes. These processes may alter the composition of marine microbial communities, affect the natural succession of microbial community structures, and disrupt the ecological niche differentiation of key functional groups. Continued studies are needed to evaluate the potential impacts of increasing OPE pollution on ocean health. The methodologies and findings of this study will help advance research on the biogeochemical cycling of emerging contaminants in the marine environment and their ecological consequences. Collectively, these results highlight that the WSCS serves as a critical region for OPE deposition, transport, and microbial-mediated transformation, with important implications for both coral reef ecosystems and deep-sea environments.

4. ENVIRONMENTAL IMPLICATIONS

Escalating emissions of OPEs constitute a significant environmental threat to the SCS, highlighting the vulnerability of marine ecosystems to emerging contaminant inputs. This study demonstrates that atmospheric deposition—primarily mediated by PM—is the dominant pathway for OPE introduction, accounting for 65.3−98.4% of total inputs. This process efficiently transports OPEs to offshore and deep-sea environments, including ecologically sensitive zones such as coral reefs. The sinking of PM facilitates the vertical transfer of OPEs, resulting in unexpected contamination of deep-sea ecosystems and introducing these pollutants into fragile food webs. Critically, microbial communities respond through functional adaptation, including taxonomic niche partitioning and upregulation of hydrolytic enzymes, representing a natural yet potentially overwhelmed mechanism for OPE degradation. These findings underscore the urgent need to regulate PM-associated emissions from regional industrial and shipping activities. Furthermore, this study establishes a paradigm for understanding the fate of particle-reactive emerging pollutants, emphasizing the coupled roles of physical transport and biological transformation in determining their environmental impact. Mitigation strategies must consider the atmosphere−surface seawater−deep-sea continuum to effectively preserve ocean health.

■ ASSOCIATED CONTENT

Supporting Information

The Supporting Information is available free of charge at https://pubs.acs.org/doi/10.1021/acs.est.5c09148.

Calculation of gas−particle partitioning; calculation of air−water exchange and deposition; and additional figures and tables (PDF)

hmwASV_Taxon_Depth_asv.full.xlsx—ASV abundance table (count matrix for all sequenced samples). MetaCyc_pathway_pred.xlsx—Predicted MetaCyc metabolic pathways based on 16S data (functional prediction results). Prediction_enzyme.xlsx—Enzyme function pre-

https://doi.org/10.1021/acs.est.5c09148
Environ. Sci. Technol. XXXX, XXX, XXX−XXX

diction based on 16S data (EC number annotation). Prediction_KO.xlsx—KEGG Orthology (KO) functional prediction based on 16S data (ZIP)

AUTHOR INFORMATION

Corresponding Author

Kefu Yu − *Guangxi Laboratory on the Study of Coral Reefs in the South China Sea, Coral Reef Research Center of China, School of Marine Sciences, Guangxi University, Nanning 530004, China; Southern Marine Science and Engineering Guangdong Laboratory (Guangzhou), Guangzhou 511458, China;* orcid.org/0000-0003-3409-9945; Phone: +86-771-3231358; Email: kefuyu@scsio.ac.cn

Authors

Minwei Han − *Guangxi Laboratory on the Study of Coral Reefs in the South China Sea, Coral Reef Research Center of China, School of Marine Sciences, Guangxi University, Nanning 530004, China;* orcid.org/0000-0001-7231-8622

Ruijie Zhang − *Guangxi Laboratory on the Study of Coral Reefs in the South China Sea, Coral Reef Research Center of China, School of Marine Sciences, Guangxi University, Nanning 530004, China;* orcid.org/0000-0002-0246-2204

Biao Chen − *Guangxi Laboratory on the Study of Coral Reefs in the South China Sea, Coral Reef Research Center of China, School of Marine Sciences, Guangxi University, Nanning 530004, China*

Mei Xiong − *Institute of Genetics and Developmental Biology, Chinese Academy of Sciences, Beijing 100101, China*

Yaru Kang − *Guangxi Laboratory on the Study of Coral Reefs in the South China Sea, Coral Reef Research Center of China, School of Marine Sciences, Guangxi University, Nanning 530004, China*

Xiaopeng Yu − *Guangxi Laboratory on the Study of Coral Reefs in the South China Sea, Coral Reef Research Center of China, School of Marine Sciences, Guangxi University, Nanning 530004, China*

Zhenjun Qin − *Guangxi Laboratory on the Study of Coral Reefs in the South China Sea, Coral Reef Research Center of China, School of Marine Sciences, Guangxi University, Nanning 530004, China*

Xiangrong Xu − *Guangxi Laboratory on the Study of Coral Reefs in the South China Sea, Coral Reef Research Center of China, School of Marine Sciences, Guangxi University, Nanning 530004, China*

Complete contact information is available at: https://pubs.acs.org/10.1021/acs.est.5c09148

Author Contributions

Minwei Han: Writing original draft, Methodology, Investigation, Formal analysis, Data curation. Kefu Yu: Supervision, Resources, Funding acquisition. Ruijie Zhang: Data curation, Methodology. Biao Chen: Investigation, Supervision, Data curation. Mei Xiong: Visualization, Image retouching, Software. Yaru Kang: Methodology, Writing—review and editing. Xiaopeng Yu: Visualization, Writing—review and editing. Zhenjun Qin: Formal analysis, Writing—review and editing. Xiangrong Xu: Formal analysis, Writing—review and editing.

Notes

The authors declare no competing financial interest.

ACKNOWLEDGMENTS

This work was supported by the National Natural Science Foundation of China (No. 42030502), Guangxi Scientific Project (No. AD25069075), and Guangxi Natural Science Foundation (No. 2025GXNSFBA069537). The work was also supported by Southern Marine Science and Engineering Guangdong Laboratory (Zhuhai) (No. SML2021SI2005).

REFERENCES

(1) Xie, Z.; Wang, P.; Wang, X.; Castro-Jiménez, J.; Kallenborn, R.; Liao, C.; Mi, W.; Lohmann, R.; Vila-Costa, M.; Dachs, J. Organophosphate ester pollution in the oceans. *Nat. Rev. Earth Environ.* **2022**, *3* (5), 309−322.

(2) Ye, L.; Su, G. Elevated concentration and high Diversity of organophosphate esters (OPEs) were Discovered in Sediment from Industrial, and E-Waste Recycling Areas. *Water Res.* **2022**, *217*, 118362.

(3) Liu, Y.; Gong, S.; Ye, L.; Li, J.; Liu, C.; Chen, D.; Fang, M.; Letcher, R. J.; Su, G. Organophosphate (OP) diesters and a review of sources, chemical properties, environmental occurrence, adverse effects, and future directions. *Environ. Int.* **2021**, *155*, 106691.

(4) Dong, C.; Zhang, G.; Pei, Z.; Yang, R.; Li, Y.; Zhang, Q.; Jiang, G. Organophosphate esters in terrestrial environments of Fildes Peninsula, Antarctica: Occurrence, potential sources, and bioaccumulation. *J. Hazard. Mater.* **2024**, *478*, 135519.

(5) Trilla-Prieto, N.; Iriarte, J.; Berrojalbiz, N.; Casas, G.; Sobrino, C.; Vila-Costa, M.; Jiménez, B.; Dachs, J. Enrichment of Organophosphate Esters in the Sea Surface Microlayer from the Atlantic and Southern Oceans. *Environ. Sci. Technol. Lett.* **2024**, *11* (9), 1008−1015.

(6) Ding, Y.; Han, M.; Wu, Z.; Zhang, R.; Li, A.; Yu, K.; Wang, Y.; Huang, W.; Zheng, X.; Mai, B. Bioaccumulation and trophic transfer of organophosphate esters in tropical marine food web, South China Sea. *Environ. Int.* **2020**, *143*, 105919.

(7) Fu, J.; Fu, K.; Chen, Y.; Li, X.; Ye, T.; Gao, K.; Pan, W.; Zhang, A.; Fu, J. Long-Range Transport, Trophic Transfer, and Ecological Risks of Organophosphate Esters in Remote Areas. *Environ. Sci. Technol.* **2021**, *55* (15), 10192−10209.

(8) Huang, Q.; Hou, R.; Lin, L.; Li, H.; Liu, S.; Cheng, Y.; Xu, X. Bioaccumulation and Trophic Transfer of Organophosphate Flame Retardants and Their Metabolites in the Estuarine Food Web of the Pearl River, China. *Environ. Sci. Technol.* **2023**, *57* (9), 3549−3561.

(9) Gu, L.; Hu, B.; Fu, Y.; Zhou, W.; Li, X.; Huang, K.; Zhang, Q.; Fu, J.; Zhang, H.; Zhang, A.; Fu, J.; Jiang, G. Occurrence and risk assessment of organophosphate esters in global aquatic products. *Water Res.* **2023**, *240*, 120083.

(10) Xie, J.; Zhang, G.; Chen, C.; Luo, M.; Xu, H.; Chen, D.; Liu, R.; Li, Y.; Zhang, Q.; Zhang, Y.; Peng, X.; He, L.; Lin, T.; Jiang, G. Tracing Organophosphate Ester Pollutants in Hadal Trenches−Distribution, Possible Origins, and Transport Mechanisms. *Environ. Sci. Technol.* **2024**, *58* (9), 4392−4403.

(11) Lao, J.-Y.; Wu, R.; Cui, Y.; Zhou, S.; Ruan, Y.; Leung, K. M. Y.; Wu, J.; Zeng, E. Y.; Lam, P. K. S. Significant input of organophosphate esters through particle-mediated transport into the Pearl River Estuary, China. *J. Hazard. Mater.* **2022**, *438*, 129486.

(12) Jepson, P. D.; Law, R. J. Persistent pollutants, persistent threats. *Science* **2016**, *352* (6292), 1388−1389.

(13) Lamb, J. B.; Willis, B. L.; Fiorenza, E. A.; Couch, C. S.; Howard, R.; Rader, D. N.; True, J. D.; Kelly, L. A.; Ahmad, A.; Jompa, J.; Harvell, C. D. Plastic waste associated with disease on coral reefs. *Science* **2018**, *359* (6374), 460−462.

(14) Trilla-Prieto, N.; Berrojalbiz, N.; Iriarte, J.; Fuentes-Lema, A.; Sobrino, C.; Vila-Costa, M.; Jiménez, B.; Dachs, J. Biogeochemical Controls on Latitudinal (42°N to 70°S) and Depth Distribution of Organophosphate Esters in the Atlantic and Southern Oceans. *Environ. Sci. Technol.* **2025**, *59* (11), 5585−5595.

(15) Iriarte, J.; Trilla-Prieto, N.; Berrojalbiz, N.; Vila-Costa, M.; Dachs, J. Bacterial Production Modulates the Persistence of Organophosphate Ester Flame Retardants and Plasticizers in the Ocean. *Environ. Sci. Technol. Lett.* **2025**, *12* (2), 158−165.

(16) Lv, S.; Tian, L.; Zhao, S.; Jones, K. C.; Chen, D.; Zhong, G.; Li, J.; Xu, B.; Peng, P. a.; Zhang, G. Aqueous secondary formation substantially contributes to hydrophilic organophosphate esters in aerosols. *Nat. Commun.* **2025**, *16* (1), 4463.
(17) Han, M.; Yu, K.; Zhang, R.; Chen, B.; Li, H.; Zhang, Z.-e.; Li, J.; Zhang, G. Sources of the Elevating Polycyclic Aromatic Hydrocarbon Pollution in the Western South China Sea and Its Environmental Implications. *Environ. Sci. Technol.* **2023**, *57* (49), 20750−20760.
(18) Liu, M.; Zheng, H.; Cai, M.; Leung, K. M. Y.; Li, Y.; Yan, M.; Zhang, Z.; Zhang, K.; Chen, M.; Ke, H. Ocean Stratification Impacts on Dissolved Polycyclic Aromatic Hydrocarbons (PAHs): From Global Observation to Deep Learning. *Environ. Sci. Technol.* **2023**, *57* (46), 18339−18349.
(19) Fang, Z.; Yang, W.; Chen, M.; Ma, H. Source and Fate of Dissolved Black Carbon in the Western South China Sea During the Southwest Monsoon Prevailing Season. *J. Geophys. Res.: Biogeosci.* **2017**, *122* (11), 2817−2830.
(20) Zhang, R.; Han, M.; Yu, K.; Kang, Y.; Wang, Y.; Huang, X.; Li, J.; Yang, Y. Distribution, fate and sources of polycyclic aromatic hydrocarbons (PAHs) in atmosphere and surface water of multiple coral reef regions from the South China Sea: A case study in spring-summer. *J. Hazard. Mater.* **2021**, *412*, 125214.
(21) Mi, L.; Xie, Z.; Zhang, L.; Waniek, J. J.; Pohlmann, T.; Mi, W.; Xu, W. Organophosphate Esters in Air and Seawater of the South China Sea: Spatial Distribution, Transport, and Air−Sea Exchange. *Environ. Health* **2023**, *1* (3), 191−202.
(22) Yu, K. Coral reefs in the South China Sea: Their response to and records on past environmental changes. *Sci. China: Earth Sci.* **2012**, *55* (8), 1217−1229.
(23) Lyu, L.; Li, J.; Huang, Q.; Liu, Q.; Yang, C.; Dong, J.; Su, H.; Zhang, S. Exploring the Hidden Threat of Organic UV Filters to Corals and Macroalgae in Coral Reef Ecosystem from Luhuitou, Sanya, China. *Environ. Sci. Technol.* **2025**, *59* (16), 8130−8139.
(24) Yuan, S.; Huang, J.; Qian, W.; Zhu, X.; Wang, S.; Jiang, X. Are Physical Sunscreens Safe for Marine Life? A Study on a Coral−Zooxanthellae Symbiotic System. *Environ. Sci. Technol.* **2023**, *57* (42), 15846−15857.
(25) Zhou, Z.; Tang, J.; Cao, X.; Wu, C.; Cai, W.; Lin, S. High Heterotrophic Plasticity of Massive Coral Porites pukoensis Contributes to Its Tolerance to Bioaccumulated Microplastics. *Environ. Sci. Technol.* **2023**, *57* (8), 3391−3401.
(26) Zhou, Y.; Li, Q.; Zhang, Q.; Yuan, M.; Zhu, X.; Li, Y.; Li, Q.; Downs, C. A.; Huang, D.; Chou, L.-M.; Zhao, H. Environmental Concentrations of Herbicide Prometryn Render Stress-Tolerant Corals Susceptible to Ocean Warming. *Environ. Sci. Technol.* **2024**, *58* (10), 4545−4557.
(27) Vuckovic, D.; Tinoco, A. I.; Ling, L.; Renicke, C.; Pringle, J. R.; Mitch, W. A. Conversion of oxybenzone sunscreen to phototoxic glucoside conjugates by sea anemones and corals. *Science* **2022**, *376* (6593), 644−648.
(28) Zhang, G.; Zhang, Y.; Mi, W.; Wang, Z.; Lai, S. Organophosphate esters in atmospheric particles and surface seawater in the western South China Sea. *Environ. Pollut.* **2022**, *292*, 118255.
(29) Casas, G.; Martinez-Varela, A.; Vila-Costa, M.; Jiménez, B.; Dachs, J. Rain Amplification of Persistent Organic Pollutants. *Environ. Sci. Technol.* **2021**, *55* (19), 12961−12972.
(30) Sun, Y.; De Silva, A. O.; St Pierre, K. A.; Muir, D. C. G.; Spencer, C.; Lehnherr, I.; MacInnis, J. J. Glacial Melt Inputs of Organophosphate Ester Flame Retardants to the Largest High Arctic Lake. *Environ. Sci. Technol.* **2020**, *54* (5), 2734−2743.
(31) Chen, S.; Zhou, Y.; Chen, Y.; Gu, J. fastp: an ultra-fast all-in-one FASTQ preprocessor. *Bioinformatics* **2018**, *34* (17), i884−i890.
(32) Bolyen, E.; Rideout, J. R.; Dillon, M. R.; Bokulich, N. A.; Abnet, C. C.; Al-Ghalith, G. A.; Alexander, H.; Alm, E. J.; Arumugam, M.; Asnicar, F.; Bai, Y.; Bisanz, J. E.; Bittinger, K.; Brejnrod, A.; Brislawn, C. J.; Brown, C. T.; Callahan, B. J.; Caraballo-Rodríguez, A. M.; Chase, J.; Cope, E. K.; Da Silva, R.; Diener, C.; Dorrestein, P. C.; Douglas, G. M.; Durall, D. M.; Duvallet, C.; Edwardson, C. F.; Ernst, M.; Estaki, M.; Fouquier, J.; Gauglitz, J. M.; Gibbons, S. M.; Gibson, D. L.; Gonzalez, A.; Gorlick, K.; Guo, J.; Hillmann, B.; Holmes, S.; Holste, H.; Huttenhower, C.; Huttley, G. A.; Janssen, S.; Jarmusch, A. K.; Jiang, L.; Kaehler, B. D.; Kang, K. B.; Keefe, C. R.; Keim, P.; Kelley, S. T.; Knights, D.; Koester, I.; Kosciolek, T.; Kreps, J.; Langille, M. G. I.; Lee, J.; Ley, R.; Liu, Y. X.; Loftfield, E.; Lozupone, C.; Maher, M.; Marotz, C.; Martin, B. D.; McDonald, D.; McIver, L. J.; Melnik, A. V.; Metcalf, J. L.; Morgan, S. C.; Morton, J. T.; Naimey, A. T.; Navas-Molina, J. A.; Nothias, L. F.; Orchanian, S. B.; Pearson, T.; Peoples, S. L.; Petras, D.; Preuss, M. L.; Pruesse, E.; Rasmussen, L. B.; Rivers, A.; Robeson, M. S., II; Rosenthal, P.; Segata, N.; Shaffer, M.; Shiffer, A.; Sinha, R.; Song, S. J.; Spear, J. R.; Swafford, A. D.; Thompson, L. R.; Torres, P. J.; Trinh, P.; Tripathi, A.; Turnbaugh, P. J.; Ul-Hasan, S.; van der Hooft, J. J. J.; Vargas, F.; Vázquez-Baeza, Y.; Vogtmann, E.; von Hippel, M.; Walters, W.; Wan, Y.; Wang, M.; Warren, J.; Weber, K. C.; Williamson, C. H. D.; Willis, A. D.; Xu, Z. Z.; Zaneveld, J. R.; Zhang, Y.; Zhu, Q.; Knight, R.; Caporaso, J. G. Reproducible, interactive, scalable and extensible microbiome data science using QIIME 2. *Nat. Biotechnol.* **2019**, *37* (8), 852−857.
(33) Callahan, B. J.; McMurdie, P. J.; Rosen, M. J.; Han, A. W.; Johnson, A. J.; Holmes, S. P. DADA2: High-resolution sample inference from Illumina amplicon data. *Nat. Methods* **2016**, *13* (7), 581−583.
(34) Bokulich, N. A.; Kaehler, B. D.; Rideout, J. R.; Dillon, M.; Bolyen, E.; Knight, R.; Huttley, G. A.; Gregory Caporaso, J. Optimizing taxonomic classification of marker-gene amplicon sequences with QIIME 2's q2-feature-classifier plugin. *Microbiome* **2018**, *6* (1), 90.
(35) Katoh, K.; Standley, D. M. MAFFT multiple sequence alignment software version 7: improvements in performance and usability. *Mol. Biol. Evol.* **2013**, *30* (4), 772−780.
(36) Nguyen, L. T.; Schmidt, H. A.; von Haeseler, A.; Minh, B. Q. IQ-TREE: a fast and effective stochastic algorithm for estimating maximum-likelihood phylogenies. *Mol. Biol. Evol.* **2015**, *32* (1), 268−274.
(37) Stegen, J. C.; Lin, X.; Fredrickson, J. K.; Konopka, A. E. Estimating and mapping ecological processes influencing microbial community assembly. *Front. Microbiol.* **2015**, *6*, 370.
(38) Segata, N.; Izard, J.; Waldron, L.; Gevers, D.; Miropolsky, L.; Garrett, W. S.; Huttenhower, C. Metagenomic biomarker discovery and explanation. *Genome Biol.* **2011**, *12* (6), R60.
(39) Douglas, G. M.; Maffei, V. J.; Zaneveld, J. R.; Yurgel, S. N.; Brown, J. R.; Taylor, C. M.; Huttenhower, C.; Langille, M. G. I. PICRUSt2 for prediction of metagenome functions. *Nat. Biotechnol.* **2020**, *38* (6), 685−688.
(40) Kanehisa, M.; Furumichi, M.; Sato, Y.; Kawashima, M.; Ishiguro-Watanabe, M. KEGG for taxonomy-based analysis of pathways and genomes. *Nucleic Acids Res.* **2023**, *51* (D1), D587−D592.
(41) Caspi, R.; Billington, R.; Keseler, I. M.; Kothari, A.; Krummenacker, M.; Midford, P. E.; Ong, W. K.; Paley, S.; Subhraveti, P.; Karp, P. D. The MetaCyc database of metabolic pathways and enzymes - a 2019 update. *Nucleic Acids Res.* **2020**, *48* (D1), D445−D453.
(42) Shi, T.; Li, R.; Fu, J.; Hou, C.; Gao, H.; Cheng, G.; Zhang, H.; Jin, S.; Kong, L.; Na, G. Fate of organophosphate esters from the Northwestern Pacific to the Southern Ocean: Occurrence, distribution, and fugacity model simulation. *J. Environ. Sci.* **2024**, *137*, 347−357.
(43) Möller, A.; Sturm, R.; Xie, Z.; Cai, M.; He, J.; Ebinghaus, R. Organophosphorus Flame Retardants and Plasticizers in Airborne Particles over the Northern Pacific and Indian Ocean toward the Polar Regions: Evidence for Global Occurrence. *Environ. Sci. Technol.* **2012**, *46* (6), 3127−3134.
(44) Castro-Jiménez, J.; González-Gaya, B.; Pizarro, M.; Casal, P.; Pizarro-Álvarez, C.; Dachs, J. Organophosphate Ester Flame Retardants and Plasticizers in the Global Oceanic Atmosphere. *Environ. Sci. Technol.* **2016**, *50* (23), 12831−12839.
(45) Li, R.; Gao, H.; Hou, C.; Fu, J.; Shi, T.; Wu, Z.; Jin, S.; Yao, Z.; Na, G.; Ma, X. Occurrence, source, and transfer fluxes of organophosphate esters in the South Pacific and Fildes Peninsula, Antarctic. *Sci. Total Environ.* **2023**, *894*, 164263.
(46) Na, G.; Hou, C.; Li, R.; Shi, Y.; Gao, H.; Jin, S.; Gao, Y.; Jiao, L.; Cai, Y. Occurrence, distribution, air-seawater exchange and atmos-

https://doi.org/10.1021/acs.est.5c09148
Environ. Sci. Technol. XXXX, XXX, XXX−XXX

pheric deposition of organophosphate esters (OPEs) from the Northwestern Pacific to the Arctic Ocean. *Mar. Pollut. Bull.* **2020**, *157*, 111243.
(47) Fu, J.; Fu, K.; Hu, B.; Zhou, W.; Fu, Y.; Gu, L.; Zhang, Q.; Zhang, A.; Fu, J.; Jiang, G. Source Identification of Organophosphate Esters through the Profiles in Proglacial and Ocean Sediments from Ny-Ålesund, the Arctic. *Environ. Sci. Technol.* **2023**, *57* (5), 1919−1929.
(48) Ma, Y.; Xie, Z.; Lohmann, R.; Mi, W.; Gao, G. Organophosphate Ester Flame Retardants and Plasticizers in Ocean Sediments from the North Pacific to the Arctic Ocean. *Environ. Sci. Technol.* **2017**, *51* (7), 3809−3815.
(49) Cong, B.; Li, S.; Liu, S.; Mi, W.; Liu, S.; Zhang, Z.; Xie, Z. Source and Distribution of Emerging and Legacy Persistent Organic Pollutants in the Basins of the Eastern Indian Ocean. *Environ. Sci. Technol.* **2022**, *56* (7), 4199−4209.
(50) Liao, C.; Kim, U.-J.; Kannan, K. Occurrence and distribution of organophosphate esters in sediment from northern Chinese coastal waters. *Sci. Total Environ.* **2020**, *704*, 135328.
(51) Wang, X.; Zhang, H.; Lin, C.-J.; Fu, X.; Zhang, Y.; Feng, X. Transboundary transport and deposition of Hg emission from springtime biomass burning in the Indo-China Peninsula. *J. Geophys. Res.: Atmos.* **2015**, *120* (18), 9758−9771.
(52) Wu, G.; Ram, K.; Fu, P.; Wang, W.; Zhang, Y.; Liu, X.; Stone, E. A.; Pradhan, B. B.; Dangol, P. M.; Panday, A. K.; Wan, X.; Bai, Z.; Kang, S.; Zhang, Q.; Cong, Z. Water-Soluble Brown Carbon in Atmospheric Aerosols from Godavari (Nepal), a Regional Representative of South Asia. *Environ. Sci. Technol.* **2019**, *53* (7), 3471−3479.
(53) Jiang, H.; Li, J.; Zhang, R.; Pansak, W.; Zhong, G.; Li, K.; Zhao, S.; Bualert, S.; Phewnil, O.; Zhang, G. Mapping the Contribution of Biomass Burning to Persistent Organic Pollutants in the Air of the Indo-China Peninsula Based on a Passive Air Monitoring Network. *Environ. Sci. Technol.* **2023**, *57* (6), 2274−2285.
(54) Witstok, J.; Shivaei, I.; Smit, R.; Maiolino, R.; Carniani, S.; Curtis-Lake, E.; Ferruit, P.; Arribas, S.; Bunker, A. J.; Cameron, A. J.; Charlot, S.; Chevallard, J.; Curti, M.; de Graaff, A.; D'Eugenio, F.; Giardino, G.; Looser, T. J.; Rawle, T.; Rodríguez del Pino, B.; Willott, C.; Alberts, S.; Baker, W. M.; Boyett, K.; Egami, E.; Eisenstein, D. J.; Endsley, R.; Hainline, K. N.; Ji, Z.; Johnson, B. D.; Kumari, N.; Lyu, J.; Nelson, E.; Perna, M.; Rieke, M.; Robertson, B. E.; Sandles, L.; Saxena, A.; Scholtz, J.; Sun, F.; Tacchella, S.; Williams, C. C.; Willmer, C. N. A. Carbonaceous dust grains seen in the first billion years of cosmic time. *Nature* **2023**, *621* (7978), 267−270.
(55) Huang, C.; Qi, X.; Zheng, J.; Zhu, R.; Shen, J. A maritime traffic route extraction method based on density-based spatial clustering of applications with noise for multi-dimensional data. *Ocean Eng.* **2023**, *268*, 113036.
(56) Shi, S.; Zhao, B. Modeled Exposure Assessment via Inhalation and Dermal Pathways to Airborne Semivolatile Organic Compounds (SVOCs) in Residences. *Environ. Sci. Technol.* **2014**, *48* (10), 5691−5699.
(57) Yaman, B.; Dumanoglu, Y.; Odabasi, M. Measurement and Modeling the Phase Partitioning of Organophosphate Esters Using Their Temperature-Dependent Octanol−Air Partition Coefficients and Vapor Pressures. *Environ. Sci. Technol.* **2020**, *54* (13), 8133−8143.
(58) Okeme, J. O.; Rodgers, T. F. M.; Jantunen, L. M.; Diamond, M. L. Examining the Gas-Particle Partitioning of Organophosphate Esters: How Reliable Are Air Measurements? *Environ. Sci. Technol.* **2018**, *52* (23), 13834−13844.
(59) Zhang, K.; Zhang, B.-Z.; Li, S.-M.; Zeng, E. Y. Regional dynamics of persistent organic pollutants (POPs) in the Pearl River Delta, China: Implications and perspectives. *Environ. Pollut.* **2011**, *159* (10), 2301−2309.
(60) Kang, Y.; Zhang, R.; Yu, K.; Han, M.; Li, H.; Yan, A.; Liu, F.; Shi, J.; Wang, Y. Organophosphate esters (OPEs) in a coral reef food web of the Xisha Islands, South China Sea: Occurrence, trophodynamic, and exposure risk. *Chemosphere* **2023**, *313*, 137652.
(61) Whitman, W. G. The two film theory of gas absorption. *Int. J. Heat Mass Transfer* **1962**, *5* (5), 429−433.
(62) Han, M.; Zhang, R.; Yu, K.; Yan, A.; Li, H.; Zhang, R.; Zeng, W.; Zhang, Z.-e.; Liu, F. Environmental fate and effects of PAHs in tropical mariculture ponds near the northern South China Sea: Rainfall plays a key role. *Sci. Total Environ.* **2022**, *847*, 157442.
(63) Sanganyado, E.; Chingono, K. E.; Gwenzi, W.; Chaukura, N.; Liu, W. Organic pollutants in deep sea: Occurrence, fate, and ecological implications. *Water Res.* **2021**, *205*, 117658.
(64) Birgul, A.; Tasdemir, Y.; Cindoruk, S. S. Atmospheric wet and dry deposition of polycyclic aromatic hydrocarbons (PAHs) determined using a modified sampler. *Atmos. Res.* **2011**, *101* (1−2), 341−353.
(65) Xie, Z.; Möller, A.; Ahrens, L.; Sturm, R.; Ebinghaus, R. Brominated Flame Retardants in Seawater and Atmosphere of the Atlantic and the Southern Ocean. *Environ. Sci. Technol.* **2011**, *45* (5), 1820−1826.
(66) González-Gaya, B.; Zúñiga-Rival, J.; Ojeda, M.-J.; Jiménez, B.; Dachs, J. Field Measurements of the Atmospheric Dry Deposition Fluxes and Velocities of Polycyclic Aromatic Hydrocarbons to the Global Oceans. *Environ. Sci. Technol.* **2014**, *48* (10), 5583−5592.
(67) Lian, M.; Lin, C.; Li, Y.; Hao, X.; Wang, A.; He, M.; Liu, X.; Ouyang, W. Distribution, partitioning, and health risk assessment of organophosphate esters in a major tributary of middle Yangtze River using Monte Carlo simulation. *Water Res.* **2022**, *219*, 118559.
(68) Wang, X.; Zhu, L.; Zhong, W.; Yang, L. Partition and source identification of organophosphate esters in the water and sediment of Taihu Lake, China. *J. Hazard. Mater.* **2018**, *360*, 43−50.
(69) Arrieta, J. M.; Mayol, E.; Hansman, R. L.; Herndl, G. J.; Dittmar, T.; Duarte, C. M. Dilution limits dissolved organic carbon utilization in the deep ocean. *Science* **2015**, *348* (6232), 331−333.
(70) Liu, M.; Zheng, H.; Li, H.; Chen, F.; Cui, B.; Lou, L.; Wang, W.; Zhang, H.; Chen, C.; Lin, H.; Jiang, Y.; Ye, J.; Yan, M.; Leung, K. M. Y.; Cai, M. Pyrogenic PAHs Have Different Biogeochemical Fates in the Eastern Indian Ocean. *Environ. Sci. Technol.* **2024**, *58* (50), 22405−22416.
(71) Westermann, L. M.; Lidbury, I.; Li, C. Y.; Wang, N.; Murphy, A. R. .; Aguilo Ferretjans, M. D. M.; Quareshy, M.; Shanmugan, M.; Torcello-Requena, A.; Silvano, E.; Zhang, Y. Z.; Blindauer, C. A.; Chen, Y.; Scanlan, D. J. Bacterial catabolism of membrane phospholipids links marine biogeochemical cycles. *Sci. Adv.* **2023**, *9* (17), No. eadf5122.
(72) Despotović, D.; Aharon, E.; Trofimyuk, O.; Dubovetskyi, A.; Cherukuri, K. P.; Ashani, Y.; Eliason, O.; Sperfeld, M.; Leader, H.; Castelli, A.; Fumagalli, L.; Savidor, A.; Levin, Y.; Longo, L. M.; Segev, E.; Tawfik, D. S. Utilization of diverse organophosphorus pollutants by marine bacteria. *Proc. Natl. Acad. Sci. U.S.A.* **2022**, *119* (32), No. e2203604119.
(73) Liu, Q.; Wang, X.; Zhou, J.; Yu, X.; Liu, M.; Li, Y.; Sun, H.; Zhu, L. Phosphorus Deficiency Promoted Hydrolysis of Organophosphate Esters in Plants: Mechanisms and Transformation Pathways. *Environ. Sci. Technol.* **2021**, *55* (14), 9895−9904.
(74) Liang, Y.; Zhou, X.; Wu, Y.; Wu, Y.; Zeng, X.; Yu, Z.; Peng, P. Meta-omics elucidates key degraders in a bacterial tris(2-butoxyethyl) phosphate (TBOEP)-degrading enrichment culture. *Water Res.* **2023**, *233*, 119774.
(75) Yan, A.; Zhang, R.; Yu, K.; Kang, Y.; Huang, X.; Hu, J.; Xie, S.; Yang, X.; Wang, J. Organophosphate esters (OPEs) in corals of the South China Sea: Occurrence, distribution, and bioaccumulation. *Sci. Total Environ.* **2024**, *927*, 172212.
(76) Zhang, L.; Xu, W.; Mi, W.; Yan, W.; Guo, T.; Zhou, F.; Miao, L.; Xie, Z. Atmospheric deposition, seasonal variation, and long-range transport of organophosphate esters on Yongxing Island, South China Sea. *Sci. Total Environ.* **2022**, *806*, 150673.
(77) Lai, S.; Xie, Z.; Song, T.; Tang, J.; Zhang, Y.; Mi, W.; Peng, J.; Zhao, Y.; Zou, S.; Ebinghaus, R. Occurrence and dry deposition of organophosphate esters in atmospheric particles over the northern South China Sea. *Chemosphere* **2015**, *127*, 195−200.
(78) Sun, H.; Mi, W.; Li, X.; Wang, S.; Yan, J.; Zhang, G. Organophosphate ester in surface water of the Pearl River and South China Sea, China: Spatial variations and ecological risks. *Chemosphere* **2024**, *361*, 142559.

https://doi.org/10.1021/acs.est.5c09148
Environ. Sci. Technol. XXXX, XXX, XXX−XXX

(79) Lian, M.; Wang, J.; Wang, B.; Xin, M.; Lin, C.; Gu, X.; He, M.; Liu, X.; Ouyang, W. Spatiotemporal variations and the ecological risks of organophosphate esters in Laizhou Bay waters between 2019 and 2021: Implying the impacts of the COVID-19 pandemic. *Water Res.* **2023**, *233*, 119783.

NOTE ADDED AFTER ASAP PUBLICATION

After this article was published ASAP October 20, 2025, a correction was made to Figure 6a. The corrected version was posted October 22, 2025.

https://doi.org/10.1021/acs.est.5c09148
Environ. Sci. Technol. XXXX, XXX, XXX−XXX